Journal of Materials Chemistry B

Accepted Manuscript

Volume 1 | Number 1 | Jan 2013 | Pages 1–100
Journal of Materials Chemistry B
Materials for biology and medicine
www.rsc.org/materialsB
ROYAL SOCIETY OF CHEMISTRY

This is an *Accepted Manuscript*, which has been through the Royal Society of Chemistry peer review process and has been accepted for publication.

Accepted Manuscripts are published online shortly after acceptance, before technical editing, formatting and proof reading. Using this free service, authors can make their results available to the community, in citable form, before we publish the edited article. We will replace this *Accepted Manuscript* with the edited and formatted *Advance Article* as soon as it is available.

You can find more information about *Accepted Manuscripts* in the Information for Authors.

Please note that technical editing may introduce minor changes to the text and/or graphics, which may alter content. The journal's standard Terms & Conditions and the Ethical guidelines still apply. In no event shall the Royal Society of Chemistry be held responsible for any errors or omissions in this *Accepted Manuscript* or any consequences arising from the use of any information it contains.

ROYAL SOCIETY OF CHEMISTRY

www.rsc.org/materialsB

Journal of
Materials Chemistry B

RSCPublishing

Paper

Cite this: DOI: 10.1039/x0xx00000x

Received 00th January 2014,
Accepted 00th January 2014

DOI: 10.1039/x0xx00000x

www.rsc.org/

Optical properties of hemicyanines with terminal amino groups and their application in near-infrared fluorescent imaging of nucleoli

Jia-Tao Miao,[a] Chen Fan,[b] Ru Sun,[*a] Yu-Jie Xu,[b] and Jian-Feng Ge[*a,c]

Long wavelength chromophores are of interest for material and biological applications. Six hemicyanine dyes (**1a**-**1f**) constructed with oxazolo-pyridinium, indolium, benzooxazolium, or benzothiazolium groups and terminal anilino groups with multiple methylenes were prepared. They all exhibited fluorescence from 600 to 850 nm with emission maxima in the near-infrared region. The Stokes shifts became larger in more polar solvents, likely as a result of the greater dipole moments and geometry relaxations in the excited states as suggested by (TD)DFT calculations. The hemicyanine dye with the benzothiazolium group (**1d**) exhibited the best photostability and thermal stability among those tested. The potential application of **1d** as a nucleic acid-staining fluorophore was evaluated. Fluorescent responses were observed from 575 to 850 nm when **1d** was titrated with commercially available DNA and RNA. Dye **1d** was also used in the selective fluorescent staining of RNA in live HeLa, KB and V79 cells. The results indicated that **1d** can be used as a near-infrared fluorescent probe for nucleolus imaging in live cells.

Introduction

Cyanine has attracted interest for its use as a functional dye in material[1-4] and biological[5-10] applications. The optical response is activated when cyanine dyes are noncovalently assembled or bound to two-helical structure of DNA, making them useful as reagents for the quantitative detection of DNA.[11, 12] Despite the numerous applications of traditional cyanine dyes, they are not photostable and have limited Stokes shifts.[13, 14] Some aminoheptamethinecyanines have large Stokes shifts (>100 nm) with high photostabilities and they have been widely used as special kinds of near-infrared (NIR) dyes for chemosensors.[15] Hemicyanines are a subgroup of cyanine dyes. Although tetramethylene hemicyanines based on pyridinium groups and some dimethylene hemicyanines are well studied for their potential applications in linear and nonlinear optical research,[16, 17] chemosensors,[18-21] and photovoltaic materials,[22-24] the optical properties and applications of hemicyanine dyes are still limited compared with normal cyanines.

RNA is one of the most important biomolecules in cellular processes, and the imaging of RNA has been of interest because the genetic code was established. To date, SYTO® RNASelect™ is the only commercial available RNA selective fluorescent probe in the green light region; however, its structure remains undisclosed. At 100 μM and 4 hours of incubation,[25] a europium complex can be used to stain the nucleoli of cells in the red light region, while a phenanthridine-ruthenium complex can be used for time-resolved imaging of RNA from 550 to 750 nm.[26] A fluorescein-phenanthridine fluorophore can be used to detect RNA by a fluorescence resonance energy transfer mechanism.[27] So the selectivity of RNA compared with DNA for the fluorophore is an important consideration when developing an RNA imaging agent.

Hemicyanines have potential applications in the detection of the nucleic acids. A C2 symmetrical carbazole based hemicyanine was reported as a two-photon probe (λ_{em} = 550–650 nm) for RNA and DNA;[28] some quinolone based hemicyanines were identified as nucleoli-selective live cell imaging probes in the green and red regions.[29] A quinolone-benzothiazole based cyanine shows a selective response toward RNA and DNA in the NIR region although its photostability requires improvement; the corresponding stable derivative incorporating a cyano group is useful for imaging in the red light region.[30] 2,4-Bis[(*E*)-*N*-methyl-2-benzothiazolium vinyl]-1-dimethylaminobenz-ene di-iodide was recently reported as an RNA probe in the NIR region with the aid of the macrocyclic molecule cucurbit[7]uril.[31] These fluorophores can be used to image both commercial DNA and RNA, while in live cells they are primarily optically activated by RNA, thus making them useful as fluorescent probes for the imaging of nucleoli. Aside from the progress in the development of nucleic acid-staining fluorophores, their solubility, stability and biocompatibility need to be improved, and only a few NIR based probes have been reported. The optical properties and potential biological applications of hemicyanines containing terminal amino groups with large Stokes shifts are reported herein.

Experimental section

Materials and instruments.

Calfthymus DNA (ct-DNA), Saccharomyces cerevisiae RNA (S. cerevisiae RNA), bovine serum albumin (BSA), DNase and RNase were obtained from Sigma Chemical Co. (USA). ^{1}H-NMR and ^{13}C-NMR spectra were recorded on a Varian 300 or 400 MHz spectrometer, and tetramethylsilane (TMS) or the solvent peaks were used for internal standard. High resolution mass spectra were recorded on a Finnigan MAT95 mass spectrometer in ESI$^+$ mode. UV–vis absorption spectra were recorded on a Shimadzu U-3900 spectrometer. Fluorescence emission spectra were performed on a HORIBA Jobin Yvon FluoroMax-4 Spectrofluorometer. Fluorescence images of cells were obtained with a Leica TCS SP5 confocal fluorescence microscope.

Synthesis of dyes

2-(4-(4-(Dimethylamino)phenyl)buta-1,3-dien-1-yl)-4-ethyloxazolo[4,5-b]pyridin-4-ium iodide (**1a**). To a mixture of **2a** (290.1 mg, 1.00 mmol) and **3a** (189.0 mg, 1.08 mmol) in methanol (3.0 mL), pyridine (1 drops) was added, and then the mixture was refluxed for 15 h. After the reaction was cooled to room temperature, the crude product was separated by filtration and the product was purified by column chromatography eluting with dichloromethane and methanol (v: v = 15: 1) to give dark purple powder, yield: 6.9%, mp 214–217 ºC; ^{1}H NMR (400 MHz, DMSO-D$_6$) δ 8.85 (d, *J* = 6.4 Hz, 1H, Ar-*H*), 8.74 (d, *J* = 8.2 Hz, 1H, Ar-*H*), 8.02 (dd, *J* = 15.0, 11.2 Hz, 1H, C*H*), 7.88 (dd, *J* = 7.9, 6.5 Hz, 1H, Ar-*H*), 7.52 (d, *J* = 8.8 Hz, 2H, 2×Ar-*H*), 7.35 (d, *J* = 15.3 Hz, 1H, C*H*), 7.18 (dd, *J* = 15.1, 11.2 Hz, 1H, C*H*), 6.85 – 6.72 (m, 3H, 2×Ar-H, C*H*), 4.76 (q, *J* = 7.3 Hz, 2H, C*H*$_2$), 3.02 (s, 6H, 2×C*H*$_3$), 1.58 (t, *J* = 7.2 Hz, 3H, C*H*$_3$). ^{13}C NMR (75 MHz, DMSO-D$_6$) δ 170.44, 151.71, 151.02, 150.05, 146.50, 138.30, 130.01, 124.76, 122.99, 121.90, 120.82, 111.97, 109.38, 50.21, 30.71, 14.87. MS (ESI$^+$) m/z: calcd for [M-I$^-$]$^+$ $C_{20}H_{22}N_3O^+$: 320.1757, found: 320.1757.

2-(4-(4-(Dimethylamino)phenyl)buta-1,3-dien-1-yl)-1,3,3-trimethyl-3H-indol-1-ium iodide (**1b**). Compound **1b** was synthesized from **3a** and **2b** in the same way as described in the synthesis of dye **1a**. The product was finally recrystallized from ethanol to give dark blue powder, yield: 58.0%, mp 222–224 ºC; ^{1}H NMR (400 MHz, DMSO-D$_6$) δ 8.36 – 8.22 (m, 1H, C*H*), 7.82–7.68 (m, 3H, 2×Ar-H, C*H*), 7.57 (dd, *J* = 13.5, 8.2 Hz, 3H, 3×Ar-*H*), 7.50 (t, *J* = 7.2 Hz, 1H, Ar-*H*), 7.36 – 7.21 (m, 1H, C*H*), 6.97 (d, *J* = 14.9 Hz, 1H, C*H*), 6.83 (d, *J* = 8.2 Hz, 2H, 2×Ar-*H*), 3.89 (s, 3H, C*H*$_3$), 3.09 (s, 6H, 2×C*H*$_3$), 1.72 (s, 6H, 2×C*H*$_3$). ^{13}C NMR (75 MHz, DMSO-D$_6$) δ 179.79, 156.60, 153.15, 152.25, 143.10, 142.45, 131.82, 129.18, 128.27, 124.28, 123.39, 123.13, 114.35, 112.74, 111.93, 51.33, 33.54, 26.38. MS (ESI$^+$) m/z: calcd for [M-I$^-$]$^+$ $C_{23}H_{27}N_2^+$: 331.2169, found: 331.2182.

2-(4-(4-(Dimethylamino)phenyl)buta-1,3-dien-1-yl)-3,5-dimethylbenzo[d]oxazol-3-ium iodide (**1c**). Compound **1c** was synthesized from **3a** and **2c** in the same way as described in the synthesis of dye **1b**. Dark purple powder, yield: 13.6%, mp: 222-224.5 ºC; ^{1}H NMR (400 MHz, DMSO-D$_6$) δ 8.07 (t, *J* = 12.8 Hz, 1H, C*H*), 7.90 – 7.78 (m, 2H, 2×Ar-*H*), 7.59 – 7.42 (m, 4H, CH, 3×Ar-*H*), 7.20 (t, *J* = 12.0 Hz, 1H, C*H*), 6.97 (d, *J* = 14.5 Hz, 1H, C*H*), 6.78 (d, *J* = 7.9 Hz, 2H, 2×Ar-*H*), 3.98 (s, 3H, C*H*$_3$), 3.04 (s, 6H, 2×C*H*$_3$), 2.50 (s, 3H, C*H*$_3$). ^{13}C NMR (101 MHz, DMSO-D$_6$) δ 162.32, 152.24, 151.91, 149.37, 145.29, 137.49, 131.37, 130.70, 128.79, 122.69, 121.42, 113.34, 112.08, 111.54, 102.49, 31.67, 21.08. MS (ESI$^+$) m/z: calcd for [M-I$^-$]$^+$ $C_{20}H_{22}N_3O^+$: 319.1810, found: 319.1800.

2-(4-(4-(Dimethylamino)phenyl)buta-1,3-dien-1-yl)-3-methylbenzo[d]thiazol-3-ium (**1d**). Compound **1d** was synthesized from **3a** and **2d** in the same way as described in the synthesis of dye **1b**. Dark green powder, yield: 48.2%, mp 238–240 ºC; ^{1}H NMR (400 MHz, DMSO-D$_6$) δ 8.32 (d, *J* = 8.1 Hz, 1H, Ar-*H*), 8.13 (d, *J* = 8.4 Hz, 1H, Ar-*H*), 7.98 (dd, J = 14.2, 11.3 Hz, 1H, C*H*), 7.80 (t, J = 7.8 Hz, 1H, Ar-*H*), 7.70 (t, *J* = 7.6 Hz, 1H, Ar-*H*), 7.54 (d, *J* = 8.3 Hz, 2H, 2×Ar-*H*), 7.46 (t, *J* = 11.7 Hz, 3H, CH, 2×Ar-*H*), 7.32 (d, *J* = 14.6 Hz, 1H, C*H*), 7.19 (dd, *J* = 14.8, 11.2 Hz, 1H, C*H*), 7.10 (d, *J* = 7.6 Hz, 2H, 2×Ar-*H*), 6.78 (d, *J* = 8.3 Hz, 2H, 2×Ar-*H*), 4.15 (s, 3H, C*H*$_3$), 3.04 (s, 6H, 2×C*H*$_3$), 2.28 (s, 3H, C*H*$_3$). ^{13}C NMR (101 MHz, CD$_3$OD) δ 172.71, 154.29, 153.83, 151.05, 143.75, 143.55, 141.77, 132.20, 130.59, 129.95, 129.17, 128.87, 127.11, 124.81, 124.65, 123.40, 116.88, 113.24, 112.06, 40.34, 35.83, 21.46. MS (ESI$^+$) m/z: calcd for [M-TsO$^-$]$^+$ $C_{20}H_{21}N_2S^+$: 321.1425, found: 321.1437.

2-(6-(4-(Dimethylamino)phenyl)hexa-1,3,5-trien-1-yl)-1,3,3-tri-methyl-3H-indol-1-ium iodide (**1e**). Compound **1e** was synthesized from **3b** and **2b** in the same way as described in the synthesis of dye **1b**. Dark blue powder, yield: 59.7%. mp 214–216 ºC; ^{1}H NMR (400 MHz, DMSO-D$_6$) δ 8.31 – 8.16 (m, 1H, C*H*), 7.78 (dd, *J* = 12.4, 7.7 Hz, 2H, 2×Ar-*H*), 7.65 – 7.48 (m, 5H, 2×Ar-*H*, 3×C*H*), 7.10 (d, *J* = 5.0 Hz, 2H, 2×Ar-*H*), 7.01 (d, *J* = 15.0 Hz, 1H, C*H*), 6.79 (m, 3H, 2×Ar-*H*, C*H*), 3.92 (s, 3H, C*H*$_3$), 3.03 (s, 6H, 2×C*H*$_3$), 1.71 (s, 6H, 2×C*H*$_3$). ^{13}C NMR (75 MHz, DMSO-D$_6$) δ 179.58, 154.95, 152.68, 151.64, 144.99, 142.92, 142.01, 130.18, 129.90, 128.83, 128.19, 123.75, 123.66, 122.73, 114.16, 112.75, 112.04, 51.10, 33.27, 25.78. MS (ESI$^+$) m/z: calcd for [M-I$^-$]$^+$ $C_{25}H_{29}N_2^+$: 357.2325, found: 357.2341.

2-(6-(4-(Dimethylamino)phenyl)hexa-1,3,5-trien-1-yl)-3-methylbenzo[d]thiazol-3-ium iodide (**1f**). Compound **1f** was synthesized from **3b** and **2d** in the same way as described in the synthesis of dye **1b**. Dark green powder, yield: 51.5%, mp 171–173 ºC; ^{1}H NMR (400 MHz, DMSO-D$_6$) δ 8.33 (d, *J* = 8.3 Hz, 1H, Ar-*H*), 8.14 (d, *J* = 8.2 Hz, 1H, Ar-*H*), 7.93 (dd, *J* = 14.3, 11.5 Hz, 1H, C*H*), 7.81 (t, *J* = 7.7 Hz, 1H, Ar-*H*), 7.71 (t, *J* = 7.5

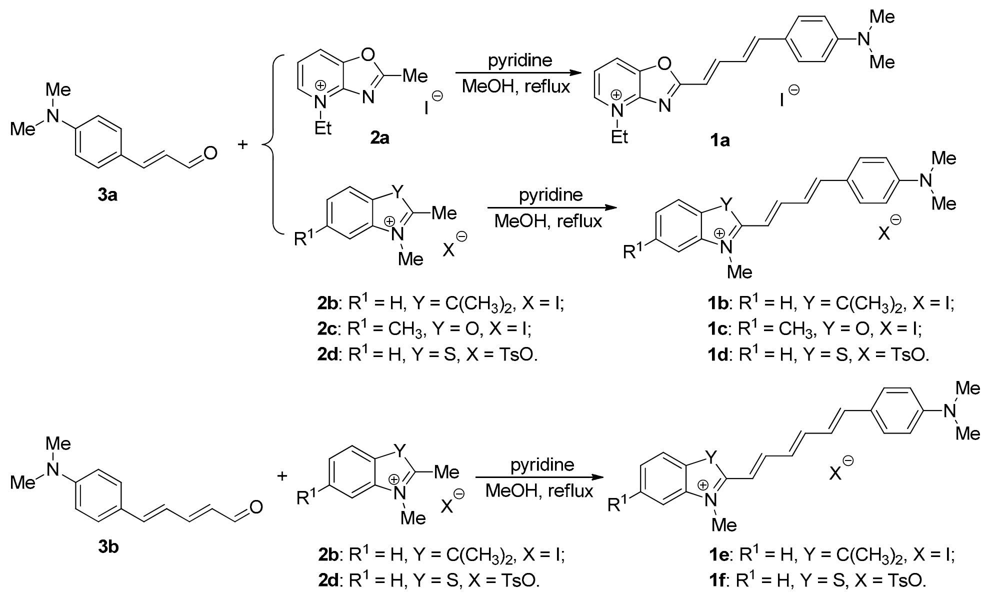
Me
N
Me
3a
+
2a
I⊖
Et
pyridine
MeOH, reflux
1a
R1
Y
Me
X⊖
2b: R1 = H, Y = C(CH3)2, X = I;
2c: R1 = CH3, Y = O, X = I;
2d: R1 = H, Y = S, X = TsO.
1b: R1 = H, Y = C(CH3)2, X = I;
1c: R1 = CH3, Y = O, X = I;
1d: R1 = H, Y = S, X = TsO.
3b
2b: R1 = H, Y = C(CH3)2, X = I;
2d: R1 = H, Y = S, X = TsO.
1e: R1 = H, Y = C(CH3)2, X = I;
1f: R1 = H, Y = S, X = TsO.

Scheme 1. Preperation of hemicyanine dyes **1a**-**f**.

Hz, 1H, Ar-H), 7.49 (t, *J* = 8.4 Hz, 4H, 2×Ar-*H*, 2×C*H*), 7.41 – 7.28 (m, 2H, 2×Ar-*H*), 7.11 (d, *J* = 7.7 Hz, 2H, 2×Ar-*H*), 7.03 (d, *J* = 8.3 Hz, 2*H*), 6.75 (t, *J* = 12.8 Hz, 3H, 2×Ar-H, C*H*), 4.17 (s, 3H, C*H*$_3$), 3.00 (s, 6H, 2×C*H*$_3$), 2.28 (s, 3H, C*H*$_3$). ^{13}C NMR (75 MHz, DMSO-D$_6$) δ 170.43, 151.09, 149.97, 148.97, 145.72, 142.65, 141.80, 137.41, 129.37, 129.00, 128.20, 127.91, 127.68, 127.26, 125.37, 123.85, 123.64, 123.43, 116.14, 113.26, 111.87, 35.50, 30.59, 20.67. MS (ESI$^+$) m/z: calcd for [M-TsO$^-$]$^+$ $C_{22}H_{23}N_2S^+$: 347.1576, found: 347.1569.

Photofading of dyes

Dyes were dissolved in ethanol with concentration of 1.0×10^{-5} M. Solutions of the samples were irradiated with a 500 W Philips iodine-tungsten lamp at room temperature. The distance between the samples and the lamp was 25 cm. A 8 cm thick cold trap (60 g/L $NaNO_2$) was set up between the 20 ml transparent glass bottle and the lamp to eliminate the heat and absorb short wavelength light. The photostability was in the terms of remaining absorption (%) calculated from the change of absorption intensity at the absorption maximum before and after irradiation.[32]

Cell culture and staining

HeLa cells, KB cells and V79 cells were cultured in Roswell Park Memorial Institute culture medium (RPMI-1640) supplemented with 10% calf serum, penicillin (100 U·mL^{-1}), streptomycin (100 μg·mL^{-1}) and L-glutamine (2.5×10^{-4} M) at 37 °C in a 5:95 CO_2-air incubator. Cells with 2×10^5 density were loaded onto a glass-bottomed coverslip with a diameter of 35 mm and cultured for 48 h before use. Hela cells were fixed by precooled methanol for 15 min, washed with PBS for 5 min twice. Deoxyri-bonuclease (DNase) and ribonuclease (RNase) digest test. Fixed HeLa cells were stained with 1 μM **1d** for 30 min. A total of 1ml clean PBS (as control experiment), 30 μg/mL DNase, or 25 μg/mL DNase-Free RNase was added into the three adjacent wells and incubated at 37 ºC in 5% CO_2 for 2 h. Cells were rinsed by clean PBS twice before imaging. Pretreated cells were stained with Hoechst 33342 (50 nM) for 30 min. After rinsing with PBS twice, the same sample was stained with **1d** (1 μM for Hela and KB cells, 0.5 μM for V79 cells) for 30 min and then imaged.

Calculation details

The geometry of the molecules at the ground state (S_0 state) and the lowest excited state (S_1 state) was optimized by density functional theory (DFT) and time-dependent DFT (TDDFT) methods with the B3LYP exchange functional employing 6-31g(d) basis sets using the Gaussian program package.[33] There are no imaginary frequencies in frequency analysis of all calculated structures; therefore, each calculated structures are in local energy minimum. The energy gap between the S_0 state and the S_1 excited state was calculated with the TDDFT method based on the optimized S_0 state geometry (for absorption) and the S_1 state geometry (for fluorescence), respectively.

Results and Discussion

Design and synthesis

The basic structures of the chromophores and auxochromes determine the absorption and emission properties of the functional dyes. Tetramethylene and hexamethylene hemicyanines were studied in this work (Scheme 1) as their longer conjugated double bonds lead to the red shift while dimethylene hemicyanines have already been well studied.[34] A terminal aniline group was selected because it creates dramatic red shifts in the known dimethylene hemicyanines compared with the normal cyanines.[1] The heterocyclic quaternary ammonium part in **1a** is used with the bioactive rhodacyanine containing oxazolopyridinium;[35] the other heterocycles, indolium, benzooxazolium, and benzothiazolium (**1b-1d**), were adopted because of their gradual red shifts as carbon, oxygen and sulfur atoms were varied in the cyanine portion.[36] Hexamethylene hemicyanines (**1e-1f**) were designed to obtain additional red shifted compounds by extension of the conjugated skeletons after the evaluation of the optical properties of the tetramethylene compounds (**1b-1d**). The D-π-A structure, which was built by expanding π-conjugation with the strong intramolecular charge transfer (ICT) from the electron-donating substituent ($C_6H_4NMe_2$) to the quaternary ammonium moiety, was adopted to construct ICT type compounds with large Stokes shifts.

The synthetic pathways are shown in Scheme 1. Compounds **2a-2d** were prepared by the alkylation of 2-methyloxazolo[4,5-*b*]pyridine, 2,3,3-trimethylindole, 2-methylbenzoxazole and 2-methylbenzothiazole, respectively.[36-38] The aldehyde (**3a-b**) can be obtained by a Wittig reaction according to reported methods.[39] The final products (**1a-1f**) were prepared by condensations between **2a-2d** and **3a-3b,** respectively, where the pyridine served as the base. The structures were fully characterized by ^1H NMR, ^{13}C NMR and HRMS analysis.

Optical properties

The normalized absorption and emission spectra of dyes **1a-1f** (10 μM) in water containing with 5% ethanol (v/v) are shown in Fig. 1. The absorption maxima of the tetramethine dyes **1a-1d** are located in the region from 501 to 577 nm. Compound **1b**, containing indolium, shows typical absorption properties of a cyanine. It has the longest absorption wavelength at 577 nm with the highest extinction coefficient, $\varepsilon = 4.6 \times 10^4\ M^{-1} \cdot cm^{-1}$, among **1a-1d**. Dyes **1a** and **1c** with oxygen atom containing heterocycles have their absorption maxima at 501 nm and 505 nm respectively. The absorption maximum was bathochromic-shifted by about 20 nm to 524 nm for the benzothiazolium containing the sulfur atom. The absorption maxima of hexamethylene dyes **1e-1f** were not much different than their corresponding tetramethine dyes **1b** and **1d** in water; however, when a less polar solvent was employed, the maximum absorption wavelengths were significantly red-shifted and higher extinction coefficients were observed (Table S1). The results indicate the electrons in the ground state are more difficult to excite in a polar solvent.

The maximum emission wavelengths of **1a-1f** are all located in the NIR region (Fig. 1, Table S1). As expected, the emission maxima of **1e-1f** (786-790 nm) in water solution are 100 nm higher than **1b-1d** because of the extension of π-conjugation from the tetramethine dyes (651-697 nm). The large Stokes shifts (107-196 nm) of **1a-1d** and the enormous Stokes shifts (222-267 nm) of **1e-1f** are observed in aqueous solution. Compared with the reported aminoheptamethine cyanines, hexamethine dyes with terminal anilino groups have similar emissions, while they have the largest reported Stokes shifts to date.[31, 40, 41] The tetramethine dyes (**1a-1d**) show low fluorescence quantum yields (0.004-0.025) in water but higher fluorescence quantum yields (0.065-0.208) in dichloromethane (Table S1). The polarity of the solvents has less of an impact on the fluorescence quantum yields of the hexamethylene dyes **1e-1f**; their weak NIR emission properties suggest a potential fluorescent enhancement application would be preferred for these types of functional dyes.

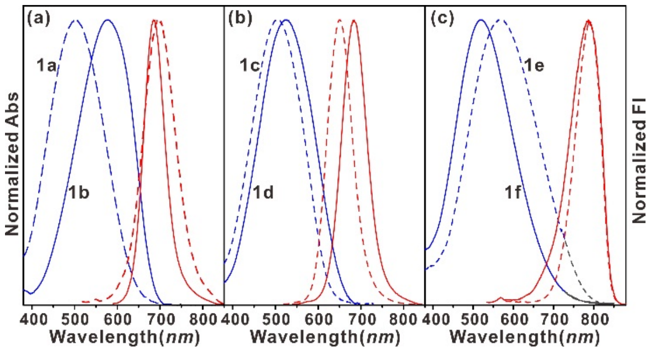

Fig. 1 Normalized absorption (blue) and normalized emission (red) spectra of dyes **1a-1f** in water/ethanol (95/5, v/v) solution. (A), **1a-1b**; (B), **1c-1d**; (C), **1e-1f**.

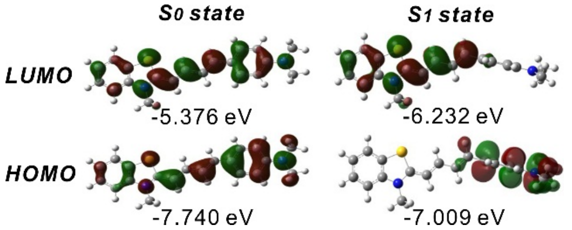

Fig. 2 The frontier molecular orbitals (FMOs) plots of dye **1d**$^+$ at the ground state (S_0 state, the left column) and the lowest excited state (S_1 state, the right column).

Rationalization of the Large Stokes Shift by (TD)DFT Calculations

As previously mentioned, the original intention of using the longer conjugated double bonds and terminal aniline groups was to shift the absorption and emission peaks to longer wavelengths. Moreover, the photophysical experiment confirmed that the Stokes shifts increase with increasing solvent polarity. An understanding of the structure–property relationship would be important for future compound design. In order to rationalize the photophysical properties of the new hemicyanine dyes **1a-1f**, especially the large Stokes shifts, the geometry of the molecules in the ground state (S_0 state) and the lowest excited state (S_1 state) were optimized by density functional theory (DFT) and time-dependent DFT (TDDFT) methods using the Gaussian program package.[33] The frontier molecular orbitals (FMOs) energy and plots, HOMO-LUMO gaps and dipole moments of dyes **1a**$^+$-**1f**$^+$ in the S_0 state and the S_1 state are shown in Fig. 2, and Tables S2 and S3.

The origin of the Stokes shifts of fluorophores can be illustrated by the simplified Jablonski diagram.[42, 43] Large geometry relaxation in the excited state (S_1 state) and changes of the energy levels of the electronic states along with geometry relaxation will produce a large Stokes shift. Conversely, small geometry relaxation or a rigid fluorophore in the excited state will produce a small Stokes shift. The geometry relaxation is the geometry difference between the energy-minimized S_0 state and the energy-minimized S_1 state. As shown in Fig. 2 and Table S3, the most prominent difference between the S_0 state geometry and the S_1 state is the dihedral angle between the aniline group and hemicyanine plane except for dye **1b**$^+$; that is, the entire molecular skeletons of **1a**$^+$ and **1c**$^+$-**1f**$^+$ in the S_0 state are on the same plane while the aniline groups in the S_1 state are hardly perpendicular to the planes of the hemicyanines accompanied by the simultaneous intramolecular charge transfer (ICT). However, no obvious change is observed for dye **1b**$^+$ after photoexcitation in order to maintain higher conjugate degree. These results indicate that planar intramolecular charge transfer (PICT) can be suggested for the optical response of **1b**$^+$,[44] while the other dyes (**1a**$^+$ and **1c**$^+$-**1f**$^+$) are following the twisted intramolecular charge transfer (TICT) mechanism.[45] This geometry relaxation upon photoexcitation impacts the energy level of the molecular orbitals. For example, the LUMO of **1d**$^+$ is stabilized by 0.856 eV in the S_1 state geometry compared with that in the S_0 state geometry, but the HOMO is destabilized by 0.731 eV (Fig. 2, Table S2). As a result, the energy gap between the HOMO and LUMO is greatly decreased with geometry relaxation in the S_1 state (0.650eV) compared with that in the S_0 state (2.109 eV). It is proposed these geometry relaxations are the main origin of the large Stokes shifts for **1a**$^+$ and **1c**$^+$-**1f**$^+$, which support the observation detailed in Table 1 that in the same solvent, **1b** exhibits the smallest Stokes shift.

It is well known that solvents strongly influence both reaction rates and the position of chemical equilibria. Such a solvent dependence is also observed for the spectral bands of individual species measured by various spectrometric techniques such as UV-visible and fluorescence spectroscopy. Shifts in absorption and emission bands can be induced by a change in solvent polarity or composition. These shifts, called solvatochromic shifts, are experimental evidence of changes in solvation energy. The energy of the emitting state of a fluorescent solute molecule is often different from that of the Franck-Condon (FC) state. One explanation for the polarity effect is a process called solvent relaxation. In most cases, the dipole moment of an aromatic molecule in the excited state, μ_e, differs from that in the ground state, μ_g. In fact, absorption of a photon by a fluorophore occurs in a very short time ($\approx$ 1fs) with respect to the displacement of the nuclei (Franck-Condon principle) but the process allows the redistribution of electrons, which results in an almost instantaneous change in the dipole moment. Most polarity probes undergo ICT upon excitation so that $\mu_e > \mu_g$ (Table S2 and S3). Taking **1d**$^+$ as an example, μ_e is calculated to be 8.6950 Debye while μ_g is 2.1520 Debye. Thus, following excitation, the solvent cage undergoes relaxation—that is, reorganization—leading to a relaxed state of minimum free energy. The higher the polarity of the solvent is, the lower the energy of the relaxed state and the larger the redshift of the emission spectrum. Therefore, exploring the photophysical properties via a theoretical perspective will be useful for the design of new fluorophores.

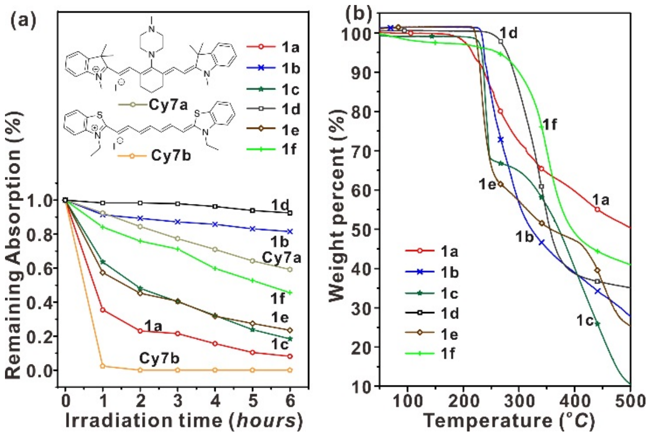

Fig. 3. (a), Photofading behaviors of dyes **1a**-**1f** and two typical Cy7 dyes in ethanol; (b), Thermal stabilities of dyes **1a**-**1f**.

Photostability and thermal stability

The photostability of cyanines **1a**–**1f** in ethanol is shown in Fig. 3(a), and the photostabilities of an aminoheptamethine-cyanine (**Cy7a**) and a traditional heptamethine cyanine without the piperazine ring (**Cy7b**) were also studied as standard samples in ethanol for comparison, as they are widely used as NIR dyes based chemo sensors. The photostability investigations of the tetramethine dyes (**1a**–**d**) indicated the benzothiazolium containing cyanine (**1d**) was the most stable one, and the indolium based hemicyanine (**1b**) also had reasonable stability. Both **1b** and **1d** were more stable than **Cy7a**, and the absorption intensities of dyes **1b** and **1d** were still over 80% in ethanol after 6 hours of irradiation while the other two tetramethine hemicyanines, **1a** and **1c**, were unstable in the same condition, decomposing rapidly by light irradiation. The indolium based hexamethine dye **1e** was also unstable and decomposed rapidly. The benzothiazolium containing hexamethine dye **1f** was slowly decomposed by irradiation and showed similar stability to **Cy7a**. **Cy7b**, another standard included for comparison, showed the worst stability and completely decomposed within one hours.

The thermogravimetric analysis (TGA) of dyes **1a**–**1f** are shown in Fig. 3(b). Compound **1a** decomposed at 190 °C, and the hexamethine dye **1f** slowly decomposed from 50°C, dyes **1b**–**1c** and **1e** decomposed around 210–230 °C, while compound **1d** was also the most stable one, starting to decompose at 250 °C.

These results indicated that the tetramethine hemicyanine **1d** is the most light and heat tolerant candidate. The cyanine dyes are electron deficient structure with positive charge, the lone pair electrons located on the sulfur atom of **1d** is greatly participated in the p-π conjugation, and the molecular system will be more stable in this case. Therefore, compound **1d** was selected for further imaging applications in next stage.

Optical responses of dye 1d towards DNA/RNA

Fluorophores with large Stokes shift and long emission wavelengths are ideal for applications as fluorescent molecular probes because of the elimination of the inner filter effect. Thus, the new hemicyanine with the terminal amino group dye described herein (**1d**) was ideal for the construction of a molecular probe. Dye **1d** had an absorption maximum at 524 nm

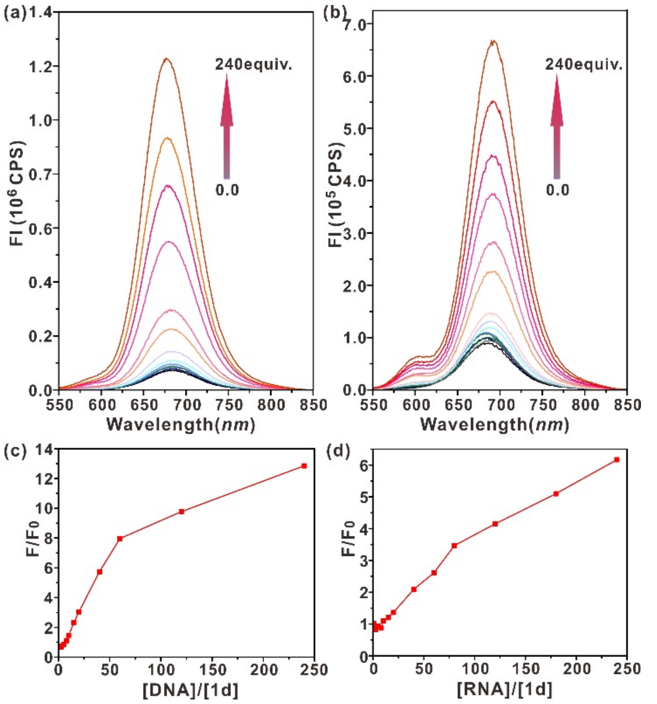

Fig. 4. Emission properties (λ_{ex} = 524 nm) of probe **1d** (5 μM) toward DNA and RNA in Tris-HCl buffer (10 mM, pH 7.4). (a, c) DNA; (b, d), RNA. (a, b), Emission spectra; (c, d), fluorescence intensity ratio versus the [NA]/[dyes] from 0 to 240, F/F_0 stand for the ratio of the fluorescence intensity at emission peaks for the final and initial states.

Table 1. Spectroscopic properties of **1d** responding to DNA and RNA.[a]

Compd.	λ_{abs}	ε^b	λ_{em}	Stokes shift	Φ^c
1d	524 nm	4.0×10^4	686 nm	162 nm	0.009
1d-DNA	547 nm	5.1×10^4	676 nm	129 nm	0.121
1d-RNA	536 nm	4.3×10^4	693 nm	157 nm	0.054

[a] Tested in Tris-HCl buffer (10 mM, pH 7.4). [b] Extinction coefficient (M^{-1}·cm^{-1}). [c] Oxazine 1 (Φ = 0.14, ethanol) was used as the reference for fluorescence quantum yields in measurements[46].

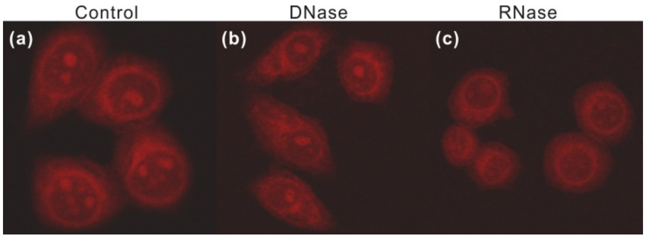

Fig. 5. Fluorescent images of the digest experiments for **1d** (1 μM) with fixed HeLa cells. (a), control, cells were incubated with **1d**; (b), cells were incubated with **1d** and DNase (30 μg/mL); (c), cells were incubated with **1d** and RNase (25 μg/mL). Images were collected in 650-795 nm with excitation at 633 nm.

with an extinction coefficient of 4.0×10^4 M^{-1}·cm^{-1} in buffer solution (Fig. S1). A titration experiment showed the absorption maximum was red-shifted to 547 nm with a higher extinction coefficient 5.1×10^4 M^{-1}·cm^{-1} when 240 equivalents of DNA was added (Fig. S1). Similarly, a quantitative spectrophotometric titration for the interaction of **1d** with 240 equivalents of RNA showed that the absorption maximum was at 536 nm with an extinction coefficient of 4.3×10^4 M^{-1}·cm^{-1} (Fig. S1).

The titration emission spectra of compound **1d** in the presence of 0 to 240 equivalents of DNA and RNA are shown in Fig. 4. It was found that **1d** showed the weak fluorescence (Φ^{free}=0.009) upon excitation at 524 nm (Fig. 4(a), Table 1). The emission maxima were slightly blue-shifted 10 nm from 686 nm to 676 nm and the emission intensities gradually increased with the sequential addition of DNA (Fig. 4(a)). The corresponding fluorescence spectra showed an approximate 12.8-fold enhancement (Fig. 4(c)) with a higher fluorescence quantum yield (Φ = 0.121), increasing 13.4-fold (Table 1). Conversely, the titration fluorescence intensity of **1d** toward RNA was enhanced by 6.2-fold with a 7 nm red shift from 686 nm to 693 nm in the presence of 240 equivalents of RNA(Fig. 4(b, d)); the fluorescence quantum yield (Φ = 0.054) was increased 6.0-fold (Table 1) upon binding to RNA. The increase of fluorescence intensity upon binding to DNA and RNA may originate from the loss of mobility in the constrictive nucleic acid environment. Moreover, the Stokes shift of **1d** were very large (129 nm with DNA and 157 nm with RNA), which could reduce self-quenching and minimize measurement errors by excitation and scattered light.

BSA was also used to study the interaction between **1d** and protein; as shown in Fig. S2, the fluorescence intensities of **1d** increased only 1.8-fold in the presence of 400 μg·mL^{-1} BSA, indicating a weak interaction between **1d** and BSA.

In cellulo fluorescent imaging

The application of compound **1d** in cell staining experiments was firstly performed with fixed-permeabilized HeLa cells, the concentration (1 μM) of probe **1d** was adopted by reported method.[30] When **1d** was incubated with fixed HeLa cells, the nucleolus of HeLa cells was stained and NIR emission was detected by fluorescent imaging (Fig. 5(a)). The selective staining of the abundant RNA nucleolus instead of the whole DNA nucleus indicated that **1d** can only noncovalently assemble with RNA in a cellular environment. Cellular DNA containing histones, which is different from the commercially available "nicked" DNA, cannot combine with **1d**. As a consequence, dye intercalation to the DNA helix structure in cells becomes more difficult than that in solution. Deoxyribonuclease (DNase) and ribonuclease (RNase) digestion tests were used to confirm the result, as DNA in the cell would be hydrolyzed in the presence of DNase while RNA would be hydrolyzed by the RNase. As shown in Fig. 5(b), there was no obvious effect on the staining after the DNase digestion test, while after RNase digestion, the fluorescence inside the nucleolus dramatically decreased (Fig.5(c)). Thus, the experiments clearly demonstrated that dye **1d** was selective for RNA in a cellular environment.

The nucleolus is the key part of the nucleus that synthesizes and assembles the ribosomal RNA, which has a significant impact on cell growth and proliferation. RNA-targeted probes is essential for live cell nucleoli imaging. Meanwhile, near-infrared (650-900 nm) fluorescent imaging have the biological advantages of optical transparency, deep tissue light penetration and minimal tissue autofluorescence. In the living cell fluorescent imaging assays, cells were first treated with the

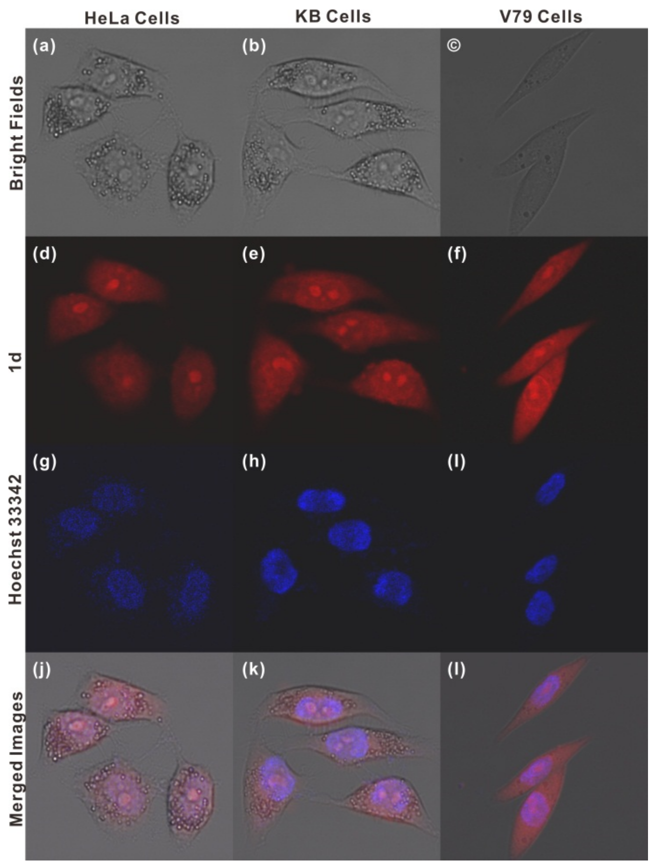

Fig. 6. Fluorescent images of nucleoli with **1d** (1 μM) in living cells. (a, d, g, j), HeLa cells; (b, e, h, k), KB cells; (c, f, i, l), V79 cells. cells. (a-c), bright fields; (d-f), cells were incubated with **1d**; (g-i), cells were incubated with Hoechst 33342 (50 nM); (j-l), merged images for each cell lines. Red chanals were collected at 650-795 nm with excitation at 633 nm, and blue channels were collected in 410-480 nm with excitation at 405 nm.

nucleus-specific dye Hoechst 33342 (50 nM) which has been widely used as a DNA marker for bio-imaging, the images of the nucleus can be obtained in the blue channel (Fig. 6(g-i), excited at 405 nm, collected from 410-480 nm). The cells were washed by PBS buffer, and then they were incubated with **1d** (1 μM for HeLa and KB cells, 0.5 μM for V79 cells) for another 30 min, and the NIR emission was observed in the red channel (excited at 633 nm, collected from 650-795 nm). As shown in Fig. 6(d-f), the fluorescence of **1d** distinguishes clear nucleoli (containing RNA) staining accompanied by faint cytoplasm (containing ribosomal RNA). The counterstain results of **1d** and Hoechst 33342 also demonstrated that the red fluorescence from the nucleolus can be easily discriminated from the nucleus zone with blue fluorescence whether it is in cancer cells or in normal cells. The reported nucleic acid or peptide based RNA probes are only has optical responses within the nucleoli parts,[47-49] probe **1d** also gives the RNA distribution in the whole cell (Fig. 6(d-f), since RNA is mainly located in nucleoli and it also partly exited in the other place of the cell.

Finally, a MTT-based colorimetric assay of compound **1d** in HeLa cells was also completed. After 6 hours of cellular internalization of the sensor at 1 μM, more than 95% of the cells were viable indicating that **1d** is not overly toxic, a key criteria for compound selection for live cell imaging. Additionally, the results from an MTT assay where the cytotoxicity of **1d** at various final concentrations (2 μM, 3 μM, 5 μM, 10 μM) was investigated, showed that the cell viability was from 94.7–98.6 % (Fig. S3). Thus, dye **1d** is a relatively low-toxic probe for live cell imaging.

Conclusions

In summary, tetramethylene and hexamethylene hemicyanine dyes (**1a**–**f**) containing terminal anilino groups were designed and synthesized and their absorption and emission properties were evaluated in different solvents. Their emissions were located in the NIR region with large Stokes shifts in water solution. (TD) DFT calculations revealed that the large Stokes shifts might be caused by the greater dipole moments and geometry relaxation in the excited state. The hemicyanine dye with the benzothiazolyl group (**1d**) showed the best photostability and thermal stability among the tested compounds. The titration experiments with **1d** and commercially available DNA/RNA gave enhanced emission at 575-850 nm. The fluorescent imaging experiments of digestion and counterstain tests showed that dye **1d** responds only toward RNA with long-wavelength excitation (633 nm) and NIR emission (650-790 nm). In particular, dye **1d** was shown to selectively stain the nucleolus of live HeLa cells, KB cells and V79 cells. In terms of its long-wave emission, large Stokes shift, water solubility, low cytotoxicity, good photostability, sensitivity and membrane permeability, probe **1d** is a good candidate for live-cell nucleolus imaging.

Acknowledgements

The project is supported from the National Natural Science Foundation of China (51273136) and the Project funded by the Priority Academic Program Development of Jiangsu Higher Education Institutions.

Notes and references

[a] *College of Chemistry, Chemical Engineering and Material Science, Collaborative Innovation Center of Suzhou Nano Science and Technology, Soochow University, 199 Ren'Ai Road, Suzhou 215123, People's Republic of China. E-mail: sunru924@hotmail.com, ge_jianfeng@hotmail.com.*

[b] *School of Radiation Medicine and Protection, Soochow University, 199 Ren'Ai Road, Suzhou 215123, People's Republic of China.*

[c] *Jiangsu Key Laboratory of Medical Optics, Suzhou Institute of Biomedical Engineering and Technology, Chinese Academy of Sciences, Suzhou 215163, China.*

† Electronic Supplementary Information (ESI) available: Related experiments and spectra. See DOI: 10.1039/b000000x/

1. H. El Ouazzani, S. Dabos-Seignon, D. Gindre, K. Iliopoulos, M. Todorova, R. Bakalska, P. Penchev, S. Sotirov, T. Kolev, V. Serbezov, A. Arbaoui, M. Bakasse and B. Sahraoui, *J. Phys. Chem. C*, 2012, **116**, 7144-7152.
2. J. M. Hales, J. Matichak, S. Barlow, S. Ohira, K. Yesudas, J. L. Bredas, J. W. Perry and S. R. Marder, *Science*, 2010, **327**, 1485-1488.
3. M. T. Spitler and B. A. Parkinson, *Acc. Chem. Res.*, 2009, **42**, 2017-2029.
4. J. T. Miao, X. Z. Wu, R. Sun, Y. L. Song and J. F. Ge, *Dyes Pigments*, 2014, **105**, 41-46.

5. M. Guillaume and B. Champagne, *Phys. Chem. Chem. Phys.*, 2005, **7**, 3284-3289.
6. B. Tang, F. Yu, P. Li, L. Tong, X. Duan, T. Xie and X. Wang, *J. Am. Chem. Soc.*, 2009, **131**, 3016-3023.
7. T. Myochin, K. Kiyose, K. Hanaoka, H. Kojima, T. Terai and T. Nagano, *J. Am. Chem. Soc.*, 2011, **133**, 3401-3409.
8. K. C. Hannah and B. A. Armitage, *Acc. Chem. Res.*, 2004, **37**, 845-853.
9. C. Flors, *Biopolymers*, 2011, **95**, 290-297.
10. N. I. Shank, H. H. Pham, A. S. Waggoner and B. A. Armitage, *J. Am. Chem. Soc.*, 2013, **135**, 242-251.
11. X. Peng, T. Wu, J. Fan, J. Wang, S. Zhang, F. Song and S. Sun, *Angew Chem. Int. Ed. Engl.*, 2011, **50**, 4180-4183.
12. T. Mahmood, A. Paul and S. Ladame, *J. Org. Chem.*, 2010, **75**, 204-207.
13. Z. Zhang and S. Achilefu, *Org. Lett.*, 2004, **6**, 2067-2070.
14. X. Peng, F. Song, E. Lu, Y. Wang, W. Zhou, J. Fan and Y. Gao, *J. Am. Chem. Soc.*, 2005, **127**, 4170-4171.
15. C. A. Bertolino, G. Caputo, C. Barolo, G. Viscardi and S. Coluccia, *J. Fluoresc.*, 2006, **16**, 221-225.
16. D. Seth, S. Sarkar, R. Pramanik, C. Ghatak, P. Setua and N. Sarkar, *J. Phys. Chem. B*, 2009, **113**, 6826-6833.
17. T. C. Pham, H. S. Kim and K. B. Yoon, *Angew Chem. Int. Ed. Engl.*, 2013, **52**, 5539-5543.
18. M. Vendrell, D. Zhai, J. C. Er and Y. T. Chang, *Chem. Rev.*, 2012, **112**, 4391-4420.
19. R. Bortolozzi, H. Ihmels, L. Thomas, M. Tian and G. Viola, *Chem-eur. J.*, 2013, **19**, 8736-8741.
20. C. Q. Zhu, S. J. Zhuo, H. Zheng, J. L. Chen, D. H. Li, S. H. Li and J. G. Xu, *Analyst*, 2004, **129**, 254-258.
21. N. Y. Kang, H. H. Ha, S. W. Yun, Y. H. Yu and Y. T. Chang, *Chem. Soc. Rev.*, 2011, **40**, 3613-3626.
22. A. Mishra, M. K. Fischer and P. Bauerle, *Angew Chem. Int. Ed. Engl.*, 2009, **48**, 2474-2499.
23. A. Hagfeldt, G. Boschloo, L. Sun, L. Kloo and H. Pettersson, *Chem. Rev.*, 2010, **110**, 6595-6663.
24. M. Cheng, X. Yang, J. Li, C. Chen, J. Zhao, Y. Wang and L. Sun, *Chem-eur. J.*, 2012, **18**, 16196-16202.
25. J. Yu, D. Parker, R. Pal, R. A. Poole and M. J. Cann, *J. Am. Chem. Soc.*, 2006, **128**, 2294-2299.
26. N. A. O'Connor, N. Stevens, D. Samaroo, M. R. Solomon, A. A. Marti, J. Dyer, H. Vishwasrao, D. L. Akins, E. R. Kandel and N. J. Turro, *Chem. Commun.*, 2009, 2640-2642.
27. N. Stevens, N. O'Connor, H. Vishwasrao, D. Samaroo, E. R. Kandel, D. L. Akins, C. M. Drain and N. J. Turro, *J. Am. Chem. Soc.*, 2008, **130**, 7182-7183.
28. X. Liu, Y. Sun, Y. Zhang, F. Miao, G. Wang, H. Zhao, X. Yu, H. Liu and W. Y. Wong, *Org. Biomol. Chem.*, 2011, **9**, 3615-3618.
29. Q. Li, Y. Kim, J. Namm, A. Kulkarni, G. R. Rosania, Y. H. Ahn and Y. T. Chang, *Chem. Biol.*, 2006, **13**, 615-623.
30. S. Zhang, J. L. Fan, Z. Y. Li, N. J. Hao, J. F. Cao, T. Wu, J. Y. Wang and X. J. Peng, *J. Mater. Chem. B*, 2014, **2**, 2688-2693.
31. Z. Li, S. Sun, Z. Yang, S. Zhang, H. Zhang, M. Hu, J. Cao, J. Wang, F. Liu, F. Song, J. Fan and X. Peng, *Biomaterials*, 2013, **34**, 6473-6481.
32. F. Song, X. Peng, E. Lu, R. Zhang, X. Chen and B. Song, *J. Photoch. Photobio. A*, 2004, **168**, 53-57.
33. M. J. Frisch, G. W. Trucks, H. B. Schlegel, G. E. Scuseria, M. A. Robb, J. R. Cheeseman, G. Scalmani, V. Barone, B. Mennucci, G. A. Petersson, H. Nakatsuji, M. Caricato, X. Li, H. P. Hratchian, A. F. Izmaylov, J. Bloino, G. Zheng, J. L. Sonnenberg, M. Hada, M. Ehara, K. Toyota, R. Fukuda, J. Hasegawa, M. Ishida, T. Nakajima, Y. Honda, O. Kitao, H. Nakai, T. Vreven, J. A. Montgomery, J. Peralta, J. E. , F. Ogliaro, M. Bearpark, J. J. Heyd, E. Brothers, K. N. Kudin, V. N. Staroverov, T. Keith, R. Kobayashi, J. Normand, K. Raghavachari, A. Rendell, J. C. Burant, S. S. Iyengar, J. Tomasi, M. Cossi, N. Rega, J. M. Millam, M. Klene, J. E. Knox, J. B. Cross, V. Bakken, C. Adamo, J. Jaramillo, R. Gomperts, R. E. Stratmann, O. Yazyev, A. J. Austin, R. Cammi, C. Pomelli, J. W. Ochterski, R. L. Martin, K. Morokuma, V. G. Zakrzewski, G. A. Voth, P. Salvador, J. J. Dannenberg, S. Dapprich, A. D. Daniels, O. Farkas, J. B. Foresman, J. V. Ortiz, J. Cioslowski and D. J. Fox, Gaussian 09, Revision C.01, Gaussian, Inc., Wallingford CT, 2010.
34. A. Mishra, R. K. Behera, P. K. Behera, B. K. Mishra and G. B. Behera, *Chem. Rev.*, 2000, **100**, 1973-2012.
35. M. Yang, C. Arai, A. Bakar Md, J. Lu, J.-F. Ge, K. Pudhom, K. Takasu, K. Kasai, M. Kaiser, R. Brun, V. Yardley, I. Itoh and M. Ihara, *J. Med. Chem.*, 2009, **53**, 368-373.
36. Q. Q. Shi, R. Sun, J. F. Ge, Q. F. Xu, N. J. Li and J. M. Lu, *Dyes Pigments*, 2012, **93**, 1506-1511.
37. K. Pudhom, K. Kasai, H. Terauchi, H. Inoue, M. Kaiser, R. Brun, M. Ihara and K. Takasu, *Bioorgan. Med. Chem.*, 2006, **14**, 8550-8563.
38. M. Panigrahi, S. Dash, S. Patel and B. K. Mishra, *Tetrahedron*, 2012, **68**, 781-805.
39. D. Plażuk, I. Janowska, A. Kłys, A. Hameed and J. Zakrzewski, *Synthetic. Commun.*, 2003, **33**, 381-385.
40. A. Mishra, R. K. Behera, P. K. Behera, B. K. Mishra and G. B. Behera, *Chem. Rev.*, 2000, **100**, 1973-2012.
41. T. Deligeorgiev, A. Vasilev, S. Kaloyanova and J. J. Vaquero, *Color. Technol.*, 2010, **126**, 55-80.
42. J. R. Lakowicz, *Principles of Fluorescence Spectroscopy*, Third Edition edn., Springer, 2006.
43. B. Valeur and M. N. Berberan-Santos, *Molecular Fluorescence*, Second Edition edn., Wiley-VCH, 2012.
44. C. A. Guido, B. Mennucci, D. Jacquemin and C. Adamo, *Phys. Chem. Chem. Phys.*, 2010, **12**, 8016-8023.
45. X. Y. Shen, W. Z. Yuan, Y. Liu, Q. Zhao, P. Lu, Y. Ma, I. D. Williams, A. Qin, J. Z. Sun and B. Z. Tang, *J. Phys. Chem. C*, 2012, **116**, 10541-10547.
46. K. Rurack and M. Spieles, *Anal. Chem.*, 2011, **83**, 1232-1242.
47. N. Nitin and G. Bao, *Bioconjugate Chem.*, 2008, **19**, 2205-2211.
48. R. W. Dirks, C. Molenaar and H. J. Tanke, *Methods*, 2003, **29**, 51-57.
49. A. S. Boutorine, D. S. Novopashina, O. A. Krasheninina, K. Nozeret and A. G. Venyaminova, *Molecules*, 2013, **18**, 15357-15397.